Handbook of

SURFACE and COLLOID CHEMISTRY

Edited by

K.S. Birdi
Royal Danish School of Pharmacy
Copenhagen, Denmark

CRC Press
Boca Raton New York

Library of Congress Cataloging-in-Publication Data

Handbook of surface and colloid chemistry / edited by K.S. Birdi.
p. cm.
Includes bibliographical references and index.
ISBN 0-8493-9459-7 (alk. paper)
1. Surface chemistry. 2. Colloids. I. Birdi, K.S., 1934–
QD508.H36 1997
541.3'3--dc21 97-3758
CIP

No claim to original U.S. Government works
International Standard Book Number 0-8493-9459-7
Library of Congress Card Number 97-3758
Printed in the United States of America 1 2 3 4 5 6 7 8 9 0
Printed on acid-free paper

13 Scattering and Absorption of Light by Particles and Aggregates

C.M. Sorensen

CONTENTS

13.1 Introduction 533
13.2 Small Particles 534
13.2.1 Polarization Considerations 534
13.2.2 The Rayleigh Differential Scattering Cross-Section 535
13.2.3 The Rayleigh Total Scattering Cross-Section 537
13.2.4 The Rayleigh Absorption Cross-Section 537
13.2.4.1 Scattering, Absorption, and Extinction 538
13.2.5 Rayleigh-Gans Scattering 539
13.3 Spheres of Arbitrary Size: The Mie Theory 539
13.3.1 The Mie Differential Scattering Cross-Sections 540
13.3.2 The Mie Total Scattering Cross-Section 542
13.4 Fractal Aggregates 543
13.4.1 Scattering and Absorption by Fractal Aggregates 545
13.4.2 The Structure Factor 546
13.5 Examples 550
Acknowledgments 554
Appendix A. Cross-Sections 554
Appendix B. The Scattering Wave Vector 555
References 557

13.1 INTRODUCTION

The goal of this review is to provide a brief yet comprehensive description of scattering and absorption of light by spherical particles of arbitrary size and aggregates of these particles that have the fractal morphology. I have refrained from derivation but have tried to give a physical interpretation of the results I quote. Exact equations for scattering and absorption are given, but the emphasis is placed not on the equations themselves but instead on the "features", i.e., important functional dependencies, relation to other forms, cardinal points, etc., and on their graphical representation. Hence, I hope I have given the reader a user's guide to light scattering and absorption that will provide a broad yet well-connected perspective which can then serve as a frame of reference for deeper studies of a particular nature.

0-8493-9459-7/97/$0.00+$.50

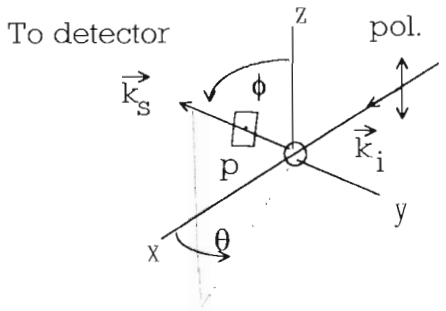

FIGURE 1 Geometry of scattering for an incident wave from the negative x-axis with propagation direction defined by the incident wave vector, $\vec{k}_i$, and with polarization (pol.) parallel to z. Light is scattered to the detector in the direction of the scattering wave vector, $\vec{k}_s$. Scattered polarization will be in the direction of the projection of the incident polarization onto the plane, p, which is perpendicular to the detector direction.

13.2 SMALL PARTICLES

Small is relative. The length scale of light is its wavelength, λ; hence, a small particle has all its dimensions small compared to λ. The simplest case, which is considered here, is a spherical particle of radius a. We may then define the size parameter as $\alpha = 2\pi a/\lambda$, which is a dimensionless ratio of the two length scales involved.

13.2.1 Polarization Considerations

With the advent of the laser, the light source of choice for light-scattering studies of colloids and aerosols has been the laser. This source is almost always polarized in the vertical plane. Thus, we will not directly discuss the case of unpolarized or natural light, such as that obtained from an ordinary light bulb or the sun, incident upon the scatterers. This can be an important situation, especially in nature, but its rules can be inferred from the incident light polarized case, which we discuss here, and it can also be found in earlier work.[1-3]

Consider a light wave traveling in the positive x direction incident upon a particle at the origin, as drawn in Figure 1. The direction of propagation is described by the incident wave vector, $\vec{k}_i$, with magnitude:

$$\left|\vec{k}_i\right| = 2\pi/\lambda \tag{1}$$

where λ is the wavelength of the light in the medium. There are two independent linear polarizations, and we shall initially consider light polarized along the z-axis. To relate this to typical laboratory situations, we will call the z-axis vertical, and the x,y plane the horizontal, scattering plane. Light can be scattered by this particle in any direction described by the scattered wave vector $\vec{k}_s$ in Figure 1. We will consider elastic scattering, hence:

$$\left|\vec{k}_s\right| = \left|\vec{k}_i\right| \tag{2}$$

For particles small compared to the wavelength we can now describe the polarization of the scattered light to be in the direction of the projection of the incident polarization onto a plane perpendicular to $\vec{k}_s$. This projection yields the amplitude of the scattered field to be proportional to $\sin\phi$, hence the scattered intensity goes as

$$I_{scat} \propto \sin^2\phi \tag{3}$$

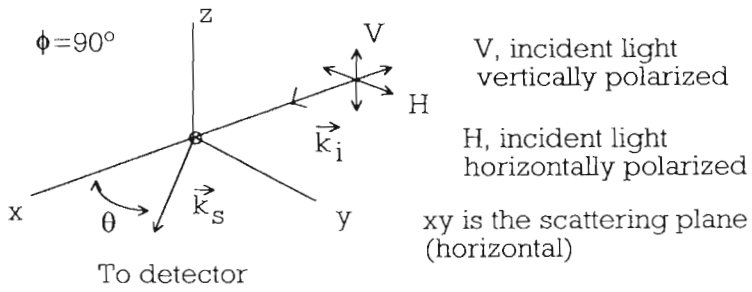

FIGURE 2 Typical scattering arrangement in which light is incident from the negative x-axis with either (or both) horizontal or vertical polarization. Scattered light is detected in the horizontal (x,y) scattering plane at a scattering angle of θ.

Most experiments are confined to the scattering plane hence $\phi = 90°$, as drawn in Figure 2. The angle, θ, is the scattering angle; $\theta = 0$ is forward scattering. We now consider incident light with polarization either vertical, V, or horizontal, H. The scattered light can be detected through a polarizer set in either the V or H directions. Thus, four scattering arrangements can be obtained, described by the scattered intensities as:

$$I_{VV}, I_{VH}, I_{HV}, \text{ and } I_{HH} \tag{4}$$

where the first subscript describes the incident polarization, the second the detected polarization of the scattered light. I_{VV} is the most common scattering arrangement, and it is the one we will describe in the rest of this review.

For particles small compared to the wavelength, these four intensities are dependent on θ in simple ways. Larger particles yield more complex functionalities but bear the imprint of the simple functionalities of their smaller brethren. The polarization rule above and the concept of projection embodied in Equation 3 can be used to infer the four intensities. The most common/scattering arrangement measures I_{VV}, which is independent of θ and isotropic in the scattering plane. The projection rule implies $I_{VH} = I_{VH} = 0$ and $I_{HH} \propto \cos^2\theta$. Figure 3 shows both a polar and cartesian plot of these functionalities.

13.2.2 The Rayleigh Differential Scattering Cross-Section

Rayleigh first presented a description of light scattering and adsorption from small particles. The conditions for Rayleigh scattering are[1-3]

$$\alpha << 1 \tag{5a}$$

$$m\alpha << 1 \tag{5b}$$

Then, the differential scattering cross-section is

$$\frac{d\sigma}{d\Omega} = k^4 a^6 \left|\frac{m^2 - 1}{m^2 + 2}\right|^2 \tag{6a}$$

$$= \frac{16\pi^4 a^6}{\lambda^4}\left|\frac{m^2 - 1}{m^2 + 2}\right|^2 \tag{6b}$$

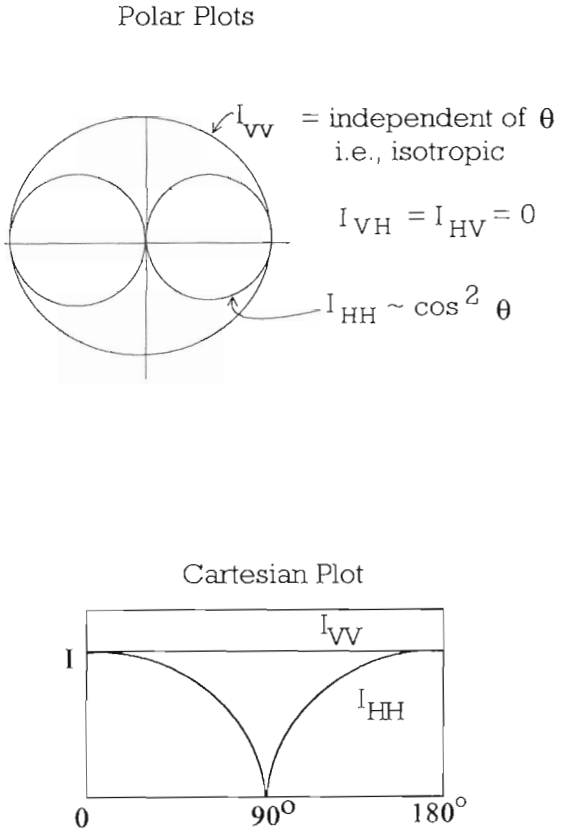

FIGURE 3 Polar and cartesian plots of Rayleigh scattering for both I_{VV} and I_{HH}.

For some elementary elaboration on the meaning of the differential scattering cross-section, the reader is referred to Appendix A. Simply put, the scattered intensity is proportional to the differential scattering cross-section. Thus, by Equation A4 and Equation 1,

$$I_{VV} = \frac{k^4 a^6}{r^2}\left|\frac{m^2-1}{m^2+2}\right|^2 I_O \tag{7}$$

Often the term involving the refractive index, the Lorentz term, is abbreviated as $F(m) = |(m^2 - 1)/(m^2 + 2)|^2$. This makes Equation 6b simply

$$\frac{d\sigma}{d\Omega} = k^4 a^6 F(m) \tag{8}$$

There are a number of important features to make note of for Rayleigh scattering:

1. The scattering is independent of θ, i.e., it is isotropic in the scattering plane. $I_{VH} = I_{HV} = 0$ and $I_{HH} = I_{VV} \cos^2 \theta$, as drawn in Figure 3.
2. The λ^{-4} dependence: Blue light scatters more than red. This is often associated with the blue of the sky and the red of the sunset,[4] but other factors are involved here, including the fact that in perfectly clean air (no particles) scattering occurs from small, thermodynamic fluctuations in the air density.
3. The strong size dependence of a^6 is proportional to the particle volume squared, V_{part}^2.

The third feature leads to the Tyndall effect,[2] which describes the increased scattering from an aggregating colloid or aerosol of constant mass. Consider that the total scattering from a particulate system of Rayleigh scatterers of n particles per unit volume has the proportionality

$$I_{scat} \propto nV_{part}^2 \tag{9}$$

If the only growth process in the system is aggregation, the mass is neither created nor destroyed. Thus, the mass density is constant, and nV_{part} is constant. On the other hand, V_{part} increases during aggregation. Rewriting Equation 9 as:

$$I_{scat} \propto nV_{part} \cdot V_{part} \tag{10}$$

shows that the scattered intensity increases proportional to V_{part} as the system aggregates. This is the Tyndall effect.

13.2.3 The Rayleigh Total Scattering Cross-Section

Integration of the differential cross-section over the complete solid angle of 4π yields the total cross-section (Equations A5 and A6). We now consider the scattering arrangement in Figure 1 with incident light polarized in the vertical direction to find:

$$\sigma = \int \frac{d\sigma}{d\Omega} d\Omega \tag{11a}$$

$$= \frac{d\sigma}{d\Omega} \int_0^{2\pi} d\theta \int_{-1}^{1} \sin^2\phi \, d(\cos\phi) \tag{11b}$$

$$= \frac{8\pi}{3} \frac{d\sigma}{d\Omega} \tag{11c}$$

We can say that the factor, $8\pi/3$, comes from integration of the polarization. Equations 8 and 11c yield:

$$\sigma_{scat} = \frac{8\pi}{3} k^4 a^6 F(m) \tag{12}$$

Thus, the scattering efficiency (Equation A7) is

$$Q_{scat} = \frac{8}{3} \alpha^4 F(m) \tag{13}$$

Note that the condition for Rayleigh scattering to hold is $\alpha << 1$; thus, Equation 13 implies that Rayleigh scatterers are not very efficient.

13.2.4 The Rayleigh Absorption Cross-Section

The Rayleigh absorption cross-section is

$$\sigma_{abs} = -\frac{8\pi^2 a^3}{\lambda} \mathrm{Im}\left(\frac{m^2 - 1}{m^2 + 2}\right) \tag{14}$$

where Im means imaginary part. We will use the notation $\mathrm{Im}[(m^2 - 1)/(m^2 + 2)] = E(m)$. Then, the absorption efficiency is simply:

$$Q_{abs} = -4\alpha E(m) \tag{15}$$

Features of Rayleigh absorption are

1. Absorption has different dependencies with λ and a than scattering:

$$\sigma_{scat} \propto \lambda^{-4} a^6$$

$$\sigma_{abs} \propto \lambda^{-1} a^3$$

$$\left(\text{a factor of } (a/\lambda)^3\right)$$

2. If m is real, there is no absorption.

13.2.4.1 Scattering, Absorption, and Extinction

When light passes through a medium containing particles, it is attenuated. This attenuation is called extinction and is described by an exponential decrease of the intensity as it passes through the medium:

$$I_{trans} = I_o e^{-\tau x} \tag{16}$$

where I_{trans} is the intensity of the light transmitted after passing a distance x through the medium, and τ is the turbidity of the medium. The turbidity is related to the number density of particles, n, and their individual extinction cross-section, σ_{ext} by:

$$\tau = n\sigma_{ext} \tag{17}$$

Extinction is due to both scattering, which removes light from the incident path, and absorption, which converts the light into other forms of energy (e.g., heat):

$$\sigma_{ext} = \sigma_{abs} + \sigma_{scat} \tag{18}$$

These facts are true for particles of all sizes, not just Rayleigh scatterers.

From the discussion above two notable features arise:

1. If m is real, extinction is solely due to scattering:

$$\sigma_{ext} = \sigma_{scat} \tag{19}$$

2. If m is complex and if the size parameter is small, $\alpha < 1$ (e.g., Rayleigh scatterers), then Equations 13 and 15 imply $\sigma_{abs} >> \sigma_{scat}$, hence:

$$\sigma_{ext} \simeq \sigma_{abs} \tag{20}$$

13.2.5 Rayleigh-Gans Scattering

The equations for Rayleigh scattering are derived under the assumption that the phase of the incident electromagnetic wave does not change across the particle. This is achieved by assuming the size of the particle to be small compared to $\lambda/2\pi$, hence the condition $\alpha << 1$ for spheres. This condition can be relaxed somewhat if the phase across the particle changes only negligibly relative to the phase change in the surrounding medium. Thus, a factor of $m - 1$ is involved, as well as the length scale, λ, and the size of the particle.

The conditions for Rayleigh-Gans scattering are

$$|m-1| << 1$$

$$2\alpha|m-1| << 1$$

Note that the second condition allows for very large particles, i.e., $\alpha > 1$, so long as m is close enough to unity to satisfy the condition.

The Rayleigh-Gans differential scattering cross-section in the scattering plane for vertically polarized light (Figure 1), is

$$\frac{d\sigma}{d\Omega_{RG}} = \frac{d\sigma}{d\Omega_R}\left[\frac{9}{u^6}(\sin u - u\cos u)^2\right] \tag{21}$$

where

$$u = 2\alpha \sin\theta/2 \tag{22a}$$

or

$$u = qa \tag{22b}$$

In Equation 21, the subscripts RG and R denote Rayleigh-Gans and Rayleigh. In Equation 22b, q is the scattering wave vector to be discussed below.

Notable features of Rayleigh-Gans scattering are

1. At $\theta = 0$, the cross-section equals the Rayleigh cross-section.
2. The scattering is larger in the forward direction, and this anisotropy increases with increasing size.

The Rayleigh-Gans absorption cross-section is equal to the Rayleigh absorption cross-section.

13.3 SPHERES OF ARBITRARY SIZE: THE MIE THEORY

The Rayleigh and Rayleigh-Gans theories of scattering and absorption represent solutions to Maxwell's equations, in which approximations could be made due to small size and small index of refraction. For an arbitrary particle, these approximations cannot be made; hence, Maxwell's equations must be solved exactly. Various symmetries, dependent on the shape of the particle, make this task more tractable, and the most symmetric (hence, simplest) is that of a homogeneous sphere, to which this discussion is limited. Mie first presented these solutions, and the term "Mie scattering" is often applied to the general description of scattering from a homogeneous sphere of arbitrary size.[1-3]

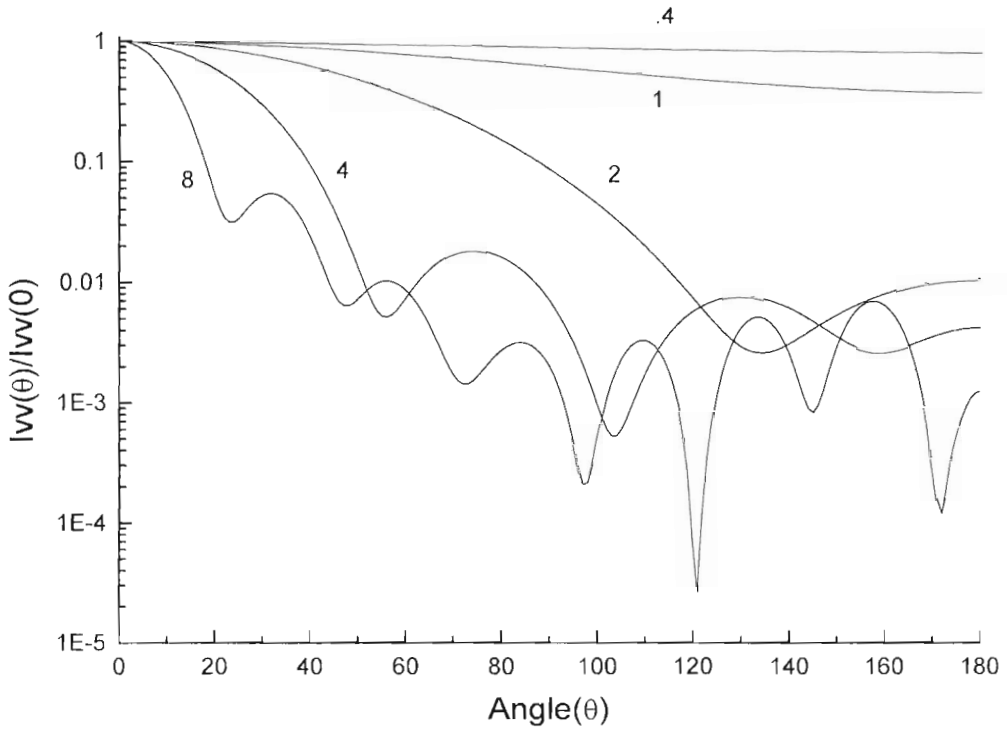

FIGURE 4 Mie Scattered intensity for vertically polarized incident and detected light as a function of scattering angle for spheres of size parameter α = 0.4, 1, 2, 4, and 8 and refractive index m = 1.33.

Mie's solution are complex enough to keep us from quoting them here. Moreover, their complexity does not allow for easy physical interpretation. Instead, we will examine the results graphically and identify important characteristics.

13.3.1 The Mie Differential Scattering Cross-Sections

Figure 4 shows the scattered intensity, I_{VV}, normalized to the intensity at $\theta = 0$ as a function of θ for m = 1.33 (e.g., H_2O drops in air) and various α. Figure 5 is similar but is for fixed $\alpha = 4.0$ and various m.

There are a number of important features to Mie scattering, many of which are illustrated in Figures 4 and 5:

1. The Mie scattering cross-section reduces to the Rayleigh limit as size approaches zero.
2. The Rayleigh-Gans theory is a good approximation up to $\alpha \simeq 1$.
3. As size increases, more scattering occurs in the forward direction.
4. As size increases, minima in the cross-section appear separated by maxima, or "Mie lobes".

Beyond these observations, the behavior of the scattered intensity or differential scattering cross-section, as seen in Figures 4 and 5, is complex. This complexity can be reduced if plots are made with the scattering wave vector, q, rather than the scattering angle, θ. The scattering wave vector, derived in Appendix B, is given by:

$$q = 4\pi\lambda^{-1} \sin\theta/2 \tag{23}$$

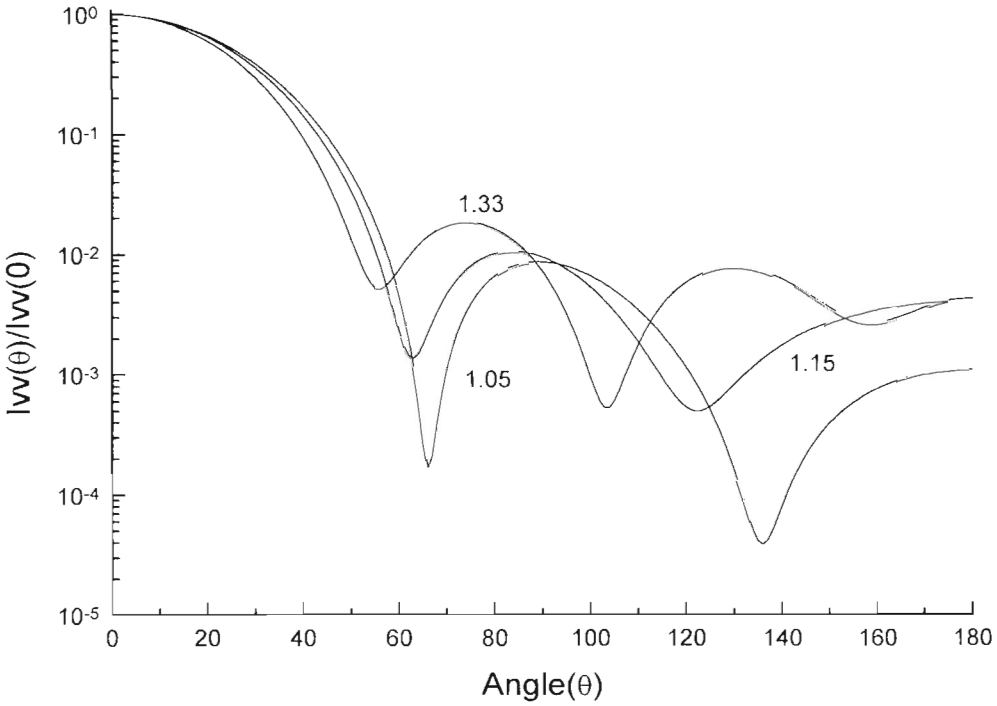

FIGURE 5 Mie scattered intensity for vertically polarized incident and detected light as a function of scattering angle for spheres of size parameter $\alpha = 4$ and refractive indices m = 1.05, 1.15, and 1.33.

Its physical significance is that the inverse, q^{-1}, is the length scale of the scattering experiment. This means that the scattering is sensitive to structures greater than q^{-1}, but it cannot "see" structures smaller than q^{-1}. Any universal character in the Mie curves should be revealed if the differential scattering cross-section is plotted vs. the ratio of the two length scales involved: the radius of the particle, a, and the length scale of the scattering experiment, q^{-1}. This ratio is the dimensionless product, qa, and both Figures 4 and 5 are replotted in Figures 6 and 7 as a function of qa.

Figures 6 and 7 display a number of important features which are listed below and represented schematically in Figure 8:

1. For $q \lesssim 1$, the Mie scattering differential cross-section has a universal behavior, i.e., independent of size, index of refraction, and shape (not shown here). This universal behavior includes:
   a. A Rayleigh regime wherein the scattering is independent of θ, and the cross-section is given by Rayleigh's equation.
   b. A regime where θ dependence first occurs and for spheres follows:

$$\frac{d\sigma}{d\Omega} = \left(\frac{d\sigma}{d\Omega}\right)_R \left(1 - \frac{1}{5}q^2a^2\right) \tag{24}$$

   This formula is readily generalized to any shape, as discussed below Equation 34.
2. The first minimum is roughly universal, lying in the region of $qa \simeq 3.8$. This corresponds well to the well-known Fraunhofer circular aperature diffraction formula:[5]

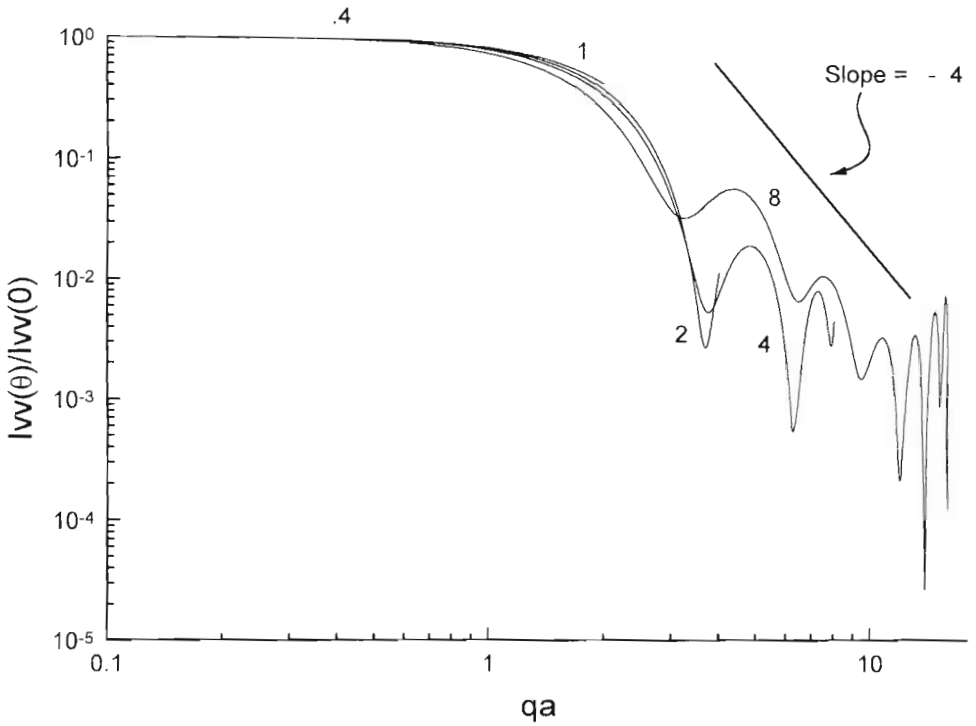

FIGURE 6 Mie scattered intensity for vertically polarized incident and detected light for spheres of size parameters $\alpha = 0.4$, 1, 2, 4, and 8 and refractive index $m = 1.33$ as a function of qa.

$$\theta \simeq 1.22\lambda/2a \tag{25}$$

3. The envelope of the $qa > 1$ regime obeys an approximate power law of q^{-4}. For scattering from mildly polydisperse systems, the minima wash out and the q^{-4} dependency remains.
4. Enhanced backscattering occurs for large particles (e.g., $\alpha = 8.0$) and is not universal on this plot.

13.3.2 The Mie Total Scattering Cross-Section

Figure 9 plots the Mie scattering efficiency as a function of the product of the size parameter and the refractive index minus one, $2\alpha(m - 1)$, the same parameter used to describe relative phase in the Rayleigh-Gans theory. This plot shows the general features but does not show the ripple structure and resonances also known to exist.[1-3] Features of the Mie scattering efficiency include:

1. Again, for small particles, $Q \sim a^4$, so $\sigma \sim a^6$.
2. A peak in the efficiency for scattering near $2\alpha(m - 1) \simeq 4.4$. For example, if $m = 1.33$, the peak is near $a \simeq \lambda$.
3. The geometric limit of Q is 2. This result is, at first, surprising if one only considers the shadow, $Q = 1$. However, edge diffraction also contributes a factor of unity, i.e.,

$$Q_{\text{geometric}} = 1(\text{shadow}) + 1(\text{edge diffraction}) \tag{26}$$

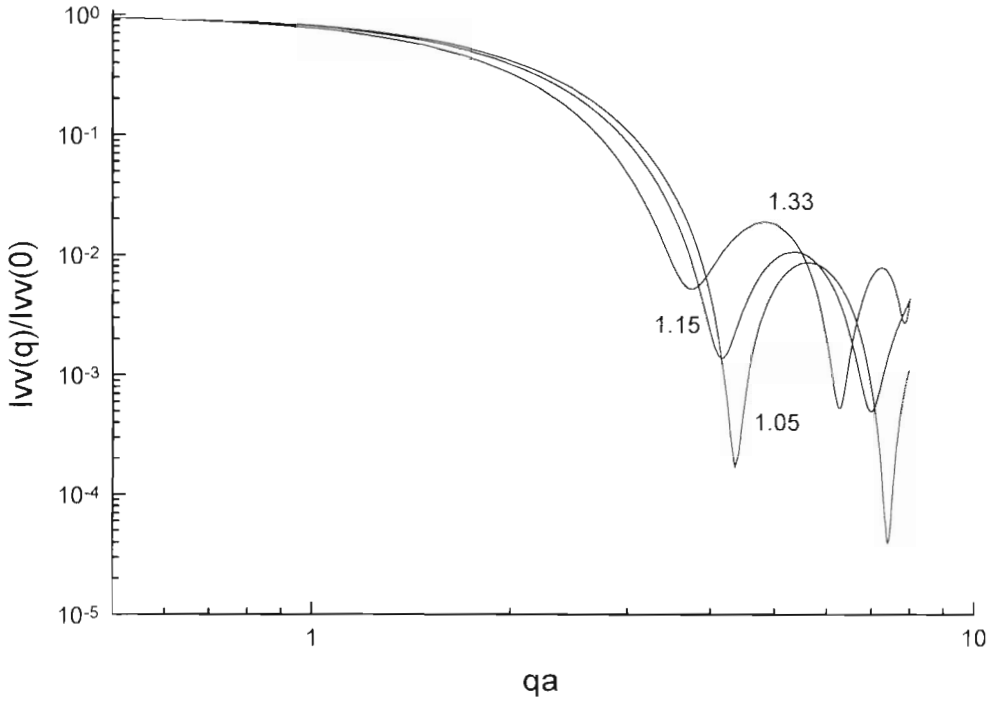

FIGURE 7 Mie scattered intensity for vertically polarized incident and detected light for spheres of size parameters $\alpha = 4$ and refractive indices m = 1.05, 1.15, and 1.33 as a function of qa.

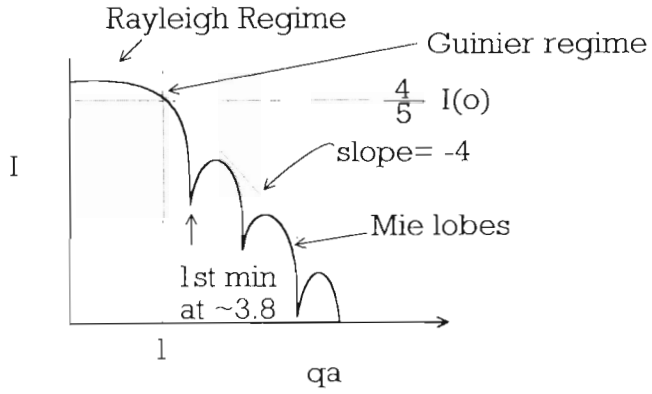

FIGURE 8 Schematic diagram of the general features of Mie scattering from a sphere.

13.4 FRACTAL AGGREGATES

The general problem of scattering and absorption by an aggregate of particles can be very complex. Much of the complexity is due to the difficulty in formulating the electromagnetic wave solution for a system that lacks symmetry and contains many scattering centers. An additional problem lies in the fact that aggregates can potentially represent an infinite number of different arrangements of constituent particles. The optics of either geometric or random assemblies of particles is an area

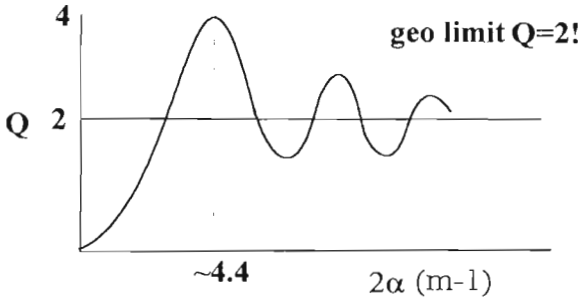

FIGURE 9 Smoothed sketch of the Mie scattering efficiency for spheres of size parameter α and refractive index m.

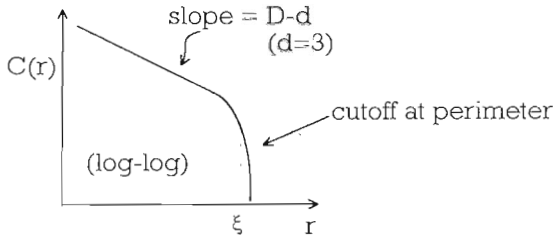

FIGURE 10 Schematic of the density autocorrelation function for a fractal aggregate.

of current active interest, especially theoretical, and the reader is referred to the literature.[6-20] Since we have little use for an infinite number of electromagnetic solutions, we need the ability to describe classes of aggregates and to quantify their features in a manner related to the scattering and absorptive behavior. The past decade and a half has seen the development of the fractal concept for the quantitative description of many aggregates that form in nature.[21-25] The scattering and absorption by fractal aggregates are now fairly well known, have an extensive literature,[26-32] and are describable in terms of the quantified fractal parameters. It is the optical properties of these fractal aggregates that are the subject of the rest of this review.

A fractal is an object that displays scale-invariant symmetry; that is, it looks the same when viewed at different scales.[21] Any real fractal object will have this scale invariance over only a finite range of scales. One important consequence of this symmetry is that the density autocorrelation function will have a power law dependence which can be written as

$$C(r) = \langle \rho(\vec{r}_o)\rho(\vec{r}_o + \vec{r})\rangle \tag{27}$$

$$= Ar^{D-d}h(r/\xi);\ r > a \tag{28}$$

Equation 27 defines the density correlation function C(r), where $\rho(\vec{r})$ is the density of material at position $\vec{r}$ and the brackets represent an ensemble average. In Equation 28, A is a normalization constant, D is the fractal dimension of the object, and d is the spatial dimension. Also in Equation 28 are the limits of scale invariance: a at the smaller scale defined by the primary or monomeric particle size, and, at the larger end of the scale, $h(r/\xi)$ is the cutoff function which governs how the density autocorrelation function (not the density itself) is terminated at the perimeter of the aggregate near the length scale, ξ. The functional behavior of C(r) is illustrated in Figure 10. Since the structure factor of scattered radiation is the Fourier transform of the density autocorrelation function, Equation 28 will be important in the development below.

Another important property of fractal aggregates is their mass scales with their sizes raised to the fractal dimension power. For a naturally occurring aggregate, apparently random to eye, size is difficult to define in terms of the typically ragged border and anisotropic shape. Thus, a convenient measure of size that can be precisely quantified is the radius of gyration, R_g, defined as:

$$R_g^2 = \int \rho(\vec{r})(\vec{r} - \vec{r}_{cm})^2 d\vec{r} / \int \rho(\vec{r}) d\vec{r} \tag{29}$$

In terms of the correlation function, one may show that R_g is given by:

$$R_g^2 = \frac{1}{2} \int r^2 C(r) d\vec{r} \tag{30}$$

In Equation 29, $\vec{r}_{cm}$ is the position of the aggregate center of mass. The radius of gyration is a root-mean-square radius, which is often a useful point of view. Given R_g, a fractal of N monomers or primary particles obeys:

$$N = k_o \left(R_g / a \right)^D \tag{31}$$

Much work has been concerned with the power law part of this important relationship, $N \sim R_g^D$, and the value of D. Only recently[33] has it been realized that the prefactor, k_o, is also an important quantity for the optical, and perhaps other, properties.[33-36]

13.4.1 Scattering and Absorption By Fractal Aggregates

To the lowest order, the scattering and absorption cross-sections for a fractal aggregate of N monomers with radius a are simply related to the monomer cross-sections as follows:[26-28]

$$\sigma_{abs}^c = N \sigma_{abs}^m \tag{32}$$

$$\frac{d\sigma^c}{d\Omega} = N^2 \frac{d\sigma^m}{d\Omega} S(q) \tag{33}$$

The superscripts c and m represent cluster and monomer, respectively. S(q) is the static structure factor of the cluster, which is the Fourier transform of the cluster density autocorrelation function and contains information regarding the cluster morphology. The structure factor has the asymptotic forms $S(0) = 1$ and $S(q) \sim q^{-D}$ for $q >> R_g^{-1}$.

The simple forms of Equations 32 and 33 have physical interpretations. Equation 32 implies that the absorption is independent of the state of aggregation; the monomers absorb independently. Equation 33 implies that the scattering at small q from N monomers is also independent of the state of aggregation, but the N scattered fields add constructively to yield the N^2 dependence of the intensity. Equations 32 and 33 are written under the assumption that the effects of intracluster multiple scattering within a cluster can be neglected. This assumption is particularly labile for $D > 2$ because such clusters are not "geometrically transparent"; that is, their projection onto a two-dimensional plane would fill the plane. Other factors that can lead to multiple scattering effects are large a (or, better, its size parameter, α), N, and m.[31] Current knowledge (see below) indicates that Equations 32 and 33 are quite good for monomer $\alpha \lesssim 0.3$, $D < 2$, and most values of m.

The general behavior of S(q) is shown in Figure 11. Important features include:

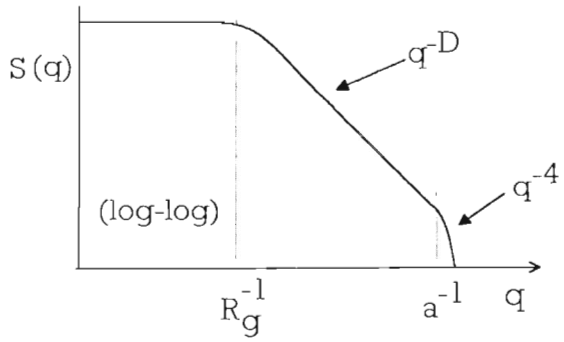

FIGURE 11 Schematic of the general behavior of the structure factor for a fractal aggregate with fractal dimension, D; radius of gyration, R_g; and monomer radius, a.

1. A scattering angle, independent Rayleigh regime where the cross-section is N^2 times the monomer Rayleigh cross-section.
2. A Guinier regime[37] near $q \sim R_g^{-1}$ which is expressed as:

$$\frac{d\sigma^2}{d\Omega} = N^2 \frac{d\sigma^m}{d\Omega}\left(1 - \frac{1}{3} q^2 R_g^2\right) \tag{34}$$

   This dependency on $q^2 R_g^2$ holds for any morphology, and Equation 34 can be used to measure the cluster R_g.
3. A power law regime at $q > R_g^{-1}$ where $S(q) \sim q^{-D}$. This can be used to measure D.
4. The regime for which $q > a^{-1}$ where the length scale of the scattering experiment can resolve below the fractal scaling regime and see the individual monomers. In this regime, $S(q) \sim q^{-4}$, as expected for Mie scattering by spheres. This feature is not included in Equation 33 but may be included by multiplying Equation 33 by the form factor, i.e., the normalized differential cross-section, for the monomer.

It is worthwhile to compare these features to those listed above for scattering from a homogeneous sphere of arbitrary size, i.e., Mie scattering. Both fractal aggregates and Mie scatterers display a Rayleigh regime in which no angle dependence occurs and for which the cross-section is proportional to the square of the amount of material present (N^2 or a^6). In each there follows, with increasing angle, a Guinier regime. Since for a uniform sphere $R_g = \sqrt{3/5}\ a$, the functional dependence is the same. After that follows a power law regime for which considerable differences appear (e.g., Mie lobes) but which are similar because of the decreasing power law with q. Finally, the possibility of enhanced back scattering for fractal aggregates, in analogy to that seen for spheres, has not to the author's knowledge been explored.

13.4.2 The Structure Factor

The structure factor and the density autocorrelation function are Fourier transform pairs; thus,

$$S(q) \propto \int C(r) e^{i\vec{q}\cdot\vec{r}} d^3r \tag{35}$$

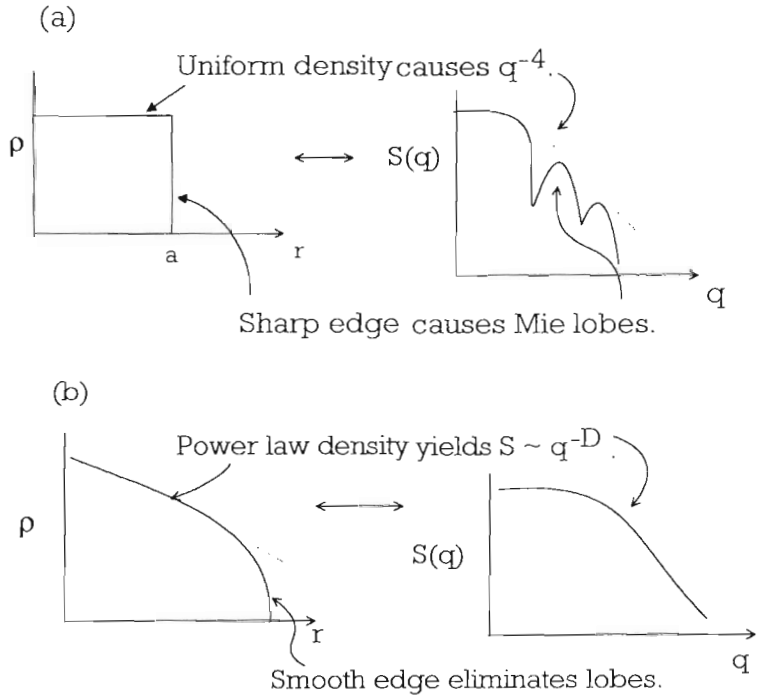

FIGURE 12 Examples of qualitative relations between particle or aggregate morphology, as described by the radial density profile, ρ vs. r, and the structure factor.

Knowledge of one implies knowledge of the other. As sure as Bragg scattering measures the structure of a crystal in q space, so, too, does the structure factor of a cluster measured optically represent the structure of the cluster in q space.

Some useful general notions of how the structure factor depends on the structure of the object from which it scatters can be obtained by considering the density profile, not the correlation function, of the object as a function of radial distance, r. This is depicted in Figure 12. A particle or cluster with uniform density and a sharp boundary (Figure 12a) is a homogeneous sphere, and its Mie scattering profile is its structure factor when $m\text{-}1 \ll 1$. The sharp boundary causes the Mie lobes, and the uniform density causes the q^{-4} envelope. If the boundary is smoothed to a finite width, the lobes become less severe, and with increasing boundary width, eventually disappear. If the density is not uniform but instead decreases with increasing r (Figure 12b), the power law describing the $qR_g > 1$ q dependence will decrease from q^{-4} to, if fractal q^{-D}, $D < 3$.

To gain more than a qualitative notion on how the structure factor is related to the structure of the object, an exact form for the correlation function must be given. A fractal object (cluster) will have $C(r) \sim r^{D-d}$, as in Equation 28. Beyond that, it is crucial to know the form of the correlation function cutoff function $h(r/\xi)$.[38-40] This function must decrease faster than any power law to effectively cut off the power law of C(r).

The early work[26-28] in this area assumed that $h(r/\xi)$ was an exponential

$$h(r/\xi) = Ae^{-(r/\xi)} \tag{36}$$

The advantages of this function are its simplicity, an analytical form for S(q) can be calculated, and it is consistent with scattering from a fluid near the critical point. Given Equation 35, a relation between R_g and ξ can be determined, and the structure factor can be calculated. These results are given in Table 1.

TABLE 1
Structure Factors and Cutoff Functions

$h(r/\xi)$	$\xi^2 =$	$S(q)$
$e^{-r/\xi}$	$\frac{2R_g^2}{D(D+1)}$	$\frac{\sin[(D-1)\tan^{-1}(q\xi)]}{(D-1)q\xi(1+q^2\xi^2)^{(D-1)/2}}$
$e^{-(r/\xi)^2}$	$\frac{4}{D}R_g^2$	$e^{-(qR_g)^2/D}\ {}_1F_1\left(\frac{3-D}{2},\frac{3}{2};\frac{(qR_g)^2}{D}\right)$ ${}_1F_1$ is the Kummer or Hypergeometric function[42]
$e^{-(r/\xi)^{2.5}}$	-	numerical[30]
Overlapping Spheres $= \left(\frac{4}{3}\pi\xi^3\right)(1+r/4\xi)$ $(1-r/2\xi)^2,\ r<2\xi$ $= 0 \qquad r>2\xi$	$\frac{(D+2)(D+5)}{2D(D+1)}R_g^2$	numerical
Fisher-Burford	$\frac{R_g^2}{3}$	$\left(1+\frac{2}{3D}q^2R_g^2\right)^{-D/2}$

An important quality of the structure factor for the exponential cutoff is that for D = 2 it reduces to the so-called Fisher-Burford formula for light scattering from a critical fluid:[41]

$$S(q) = \left(1+\frac{1}{3}q^2R_g^2\right)^{-1} \tag{37a}$$

which is often generalized for D near 2 to:

$$S(q) = \left(1+\frac{2}{3D}q^2R_g^2\right)^{-D/2} \tag{37b}$$

The beauty of these equations is their simplicity, but care must be taken because it appears that the exponential cutoff is incorrect.

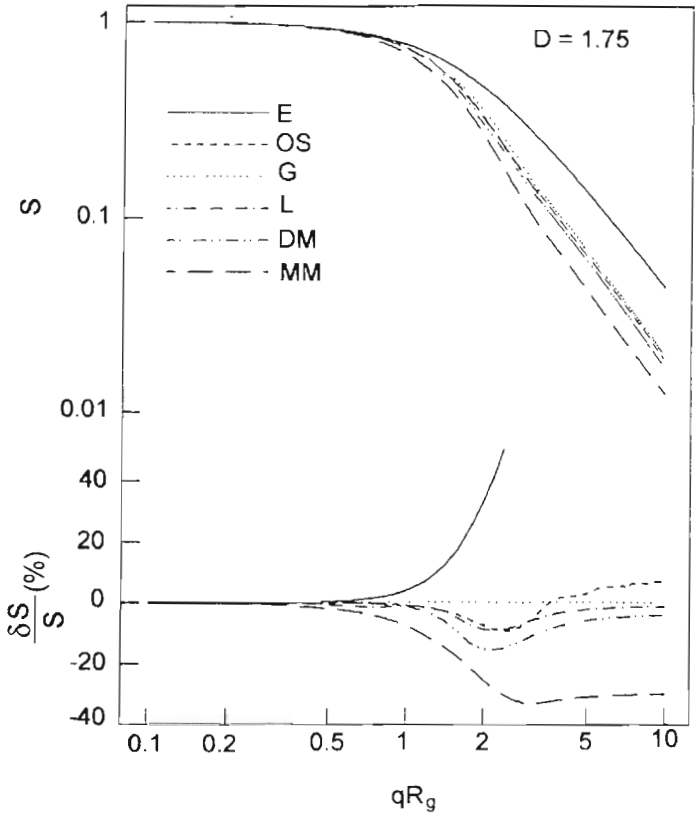

FIGURE 13 Graphical comparison of various structure factors: E = exponential, G = Gaussian; MM = Mountain and Mulholland; DM = Dobbins and Megaridis; L = Lin, et al.; OS = overlapping spheres. (From Sorensen, C. M., Cai, J., and Lu, N., Test of structure factors for describing light scattering from fractal soot aggregates, *Langmuir*, 8, 2064, 1992. With permission from American Chemical Society.)

Another reasonable form for the cutoff is the Gaussian:

$$h(r/\xi) = Ae^{-(r/\xi)^2} \tag{38}$$

Its R_g and structure factor are also included in Table 1. A cutoff based on physical reasoning is the overlapping spheres cutoff, so named because calculation of C(r) depends on how the spherical densities, $\rho(r)$, overlap.[37,39,40,43] This is also given in Table 1. Despite its physical basis, the major disadvantage of this form is the lack of an analytic form for the structure factor. Lastly, we remark that Equations 36 and 38 can be generalized to:

$$h(r/\xi) = Ae^{(-r/\xi)^\beta} \tag{39}$$

with β any positive, nonzero value. Mountain and Mulholland[30] found $\beta = 2.5 \pm 0.5$, consistent with their computer-generated clusters with D = 1.8.

Figure 13 compares these structure factors for clusters with D = 1.75 along with two other structure factors: one proposed by Lin et al.,[44] a series expansion, and one proposed by Dobbins and Megaridis,[45] based on a Guinier regime to power law regime continuity; however, neither is based on a cutoff function and are not included in Table 1. One sees that the exponential cutoff-derived structure factor stands off by itself.

In our lab we have attempted to discern which structure factor (hence, which cutoff function) describes reality the best. In one study,[38] we fit structure factor measurements from soot aggregates in a premixed CH_4/O_2 flame to the exponential, Gaussian, and Mountain and Mulholland forms, i.e., Equation 39 with $\beta = 1$, 2, and 2.5. If no polydispersity was included in the fit, $\beta = 1$ worked the best. However, with any reasonable polydispersity, $\beta = 1$, the exponential, failed completely. Both $\beta = 2$ and 2.5 worked well, with $\beta = 2$ (the Gaussian) yielding the best result.

In another study,[34] soot from the same flame was thermophoretically captured and examined via transmission electron microscopy. The correlation function of soot clusters was determined and the cutoff function extracted from that. Once again, the $\beta = 1$ exponential failed completely. The best cutoff was the overlapping spheres, which is edifying given its physical origin. However, the $\beta = 2$ Gaussian worked very well, failing only when $h(r/\xi)$ had decreased by a factor of 100.

Our conclusion is that, given the accuracy and facility of the Gaussian structure factor, it is the function that should be used in any careful analysis of scattering from fractals. Although the overlapping spheres function may be slightly better, its use is severely hindered by the lack of an analytic form for the structure factor. The exponential structure factor and, in particular, the generalized Fisher-Burford form (37b) is attractive and useful because of its simplicity. Unfortunately, part of the simplicity is that one can assume a monodisperse cluster size distribution, which is unrealistic.

Finally, one question that might arise is how the q^{-D} behavior for an aggregate transforms to q^{-4} as $D \rightarrow 3$ from below. Jullien has studied this question for both the exponential and Gaussian cutoffs.[46] For the exponential cutoff, there is an inflection in S(q) after the Guinier regime. For q less than this inflection, the negative slope on a log S(q) vs. log q plot is greater than D and approaches 4 as $D \rightarrow 3$. For q greater than the inflection q, the negative slope is equal to D. As $D \rightarrow 3$, the inflection q goes to infinity. For the Gaussian cutoff a noticeable hump appears in log S vs. q as $D \rightarrow 3$. This hump has an exponential form: $2\exp[-q^2R_g^2/3)$. At larger q, the curve inflects and begins q^{-D} behavior, i.e., the slope is –D. As $D \rightarrow 3$, the inflection point goes to infinity, leaving the exponential.

13.5 EXAMPLES

The examples given here reflect my personal research interests over the past few years regarding the morphology, optics, and physical properties of soot. Figure 14 shows a transmission electron microscope (TEM) picture of soot clusters sampled from an acetylene-in-air diffusion flame. Analysis shows these clusters are fractals with $D \simeq 1.8$ and $a = 23$ nm (thus, for $\lambda = 514.5$ nm, $\alpha = 0.28$). This is typical of carbonaceous soot formed in a variety of flames. Early work to measure and explain scattering from fractals was for colloidal systems, e.g., silica.[41] This work was concerned with the structure factor and the value of D that can be determined from the large qR_g dependence. Currently, there seems to be more work with the soot aerosols than with colloids, and it is unlike the earlier colloid work in two aspects: both absolute measurements of the scattered intensity and absorption measurements are being made. Thus, for the first time, an experimental test of fractal optics (Equations 32 and 33) can be made. As we will see, the equations are successful, but accurate comparison is currently hampered by an inaccurate knowledge of the soot refractive index, which has a value somewhere near $m = 1.6 + 0.6i$.[47]

Examples of optical structure factor measurements from aerosol soot fractal aggregates are shown in Figures 15 and 16. Figure 15 is for scattering from soot in a uniform, premixed flame of methane and oxygen.[48] As the height above the burner increases from 8 to 20 mm, the scattering goes from isotropic to angle dependent. Figure 17 shows the inverse scattered intensity, normalized to the intensity scattered at zero angle vs. wave vector squared for the data in Figure 15. The linearity is in accord with the Guinier formula (Equation 34), and the slope is $R_g^2/3$. This is a very convenient way to determine the average R_g for any system of scatterers and is the essence of the Zimm plot of biophysics.[49] Recently it has been shown that curvature of these plots in the regime of $qR_g \gtrsim 1$ can be used to measure size-distribution width.[50]

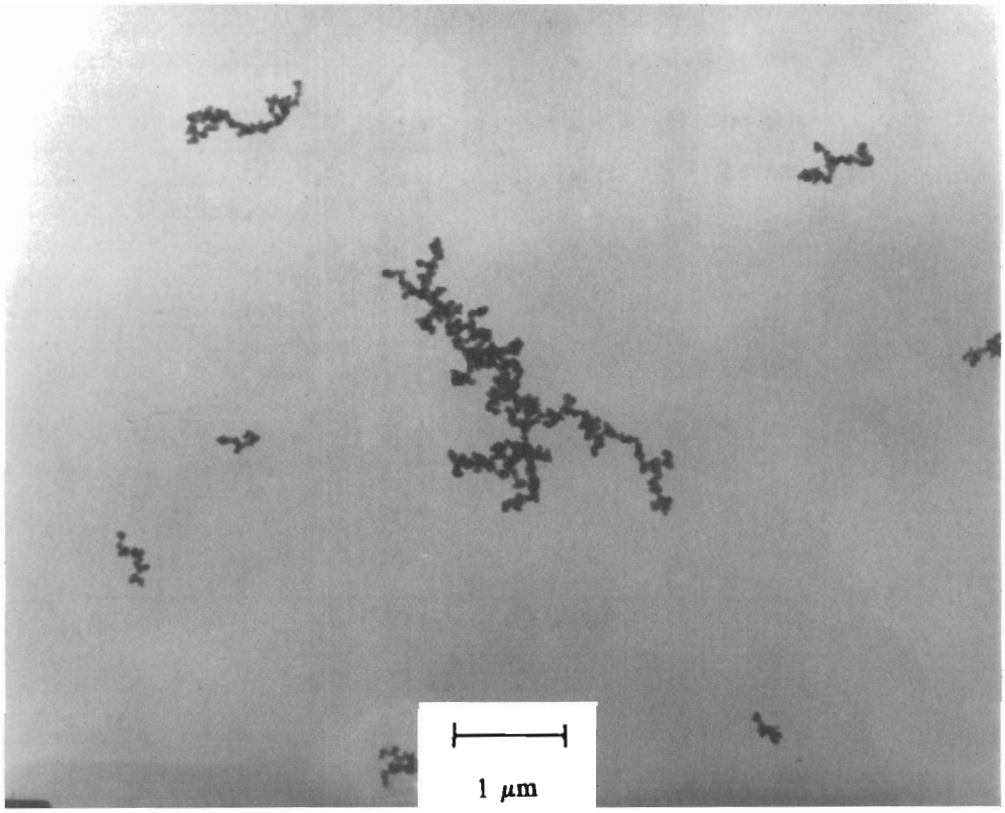

FIGURE 14 TEM micrograph of soot collected from a C_2H_2/air-diffusion flame.

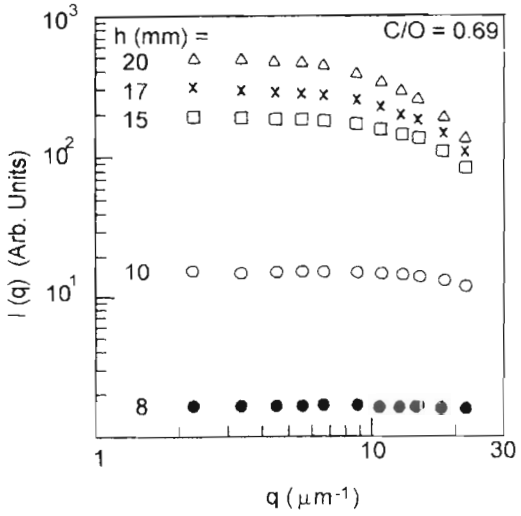

FIGURE 15 Optical structure factors for soot aggregates in a premixed CH_4/O_2 flame at various heights above burner, h. C/O is the atomic carbon to oxygen ratio.

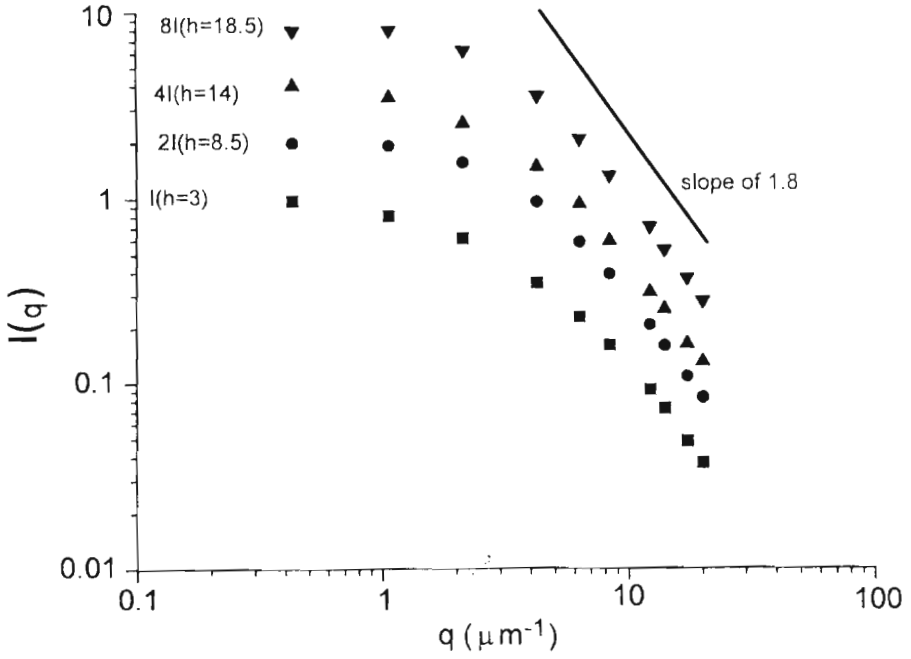

FIGURE 16 Optical structure factors for a C_2H_2/air-diffusion flame at various heights above burner, h.

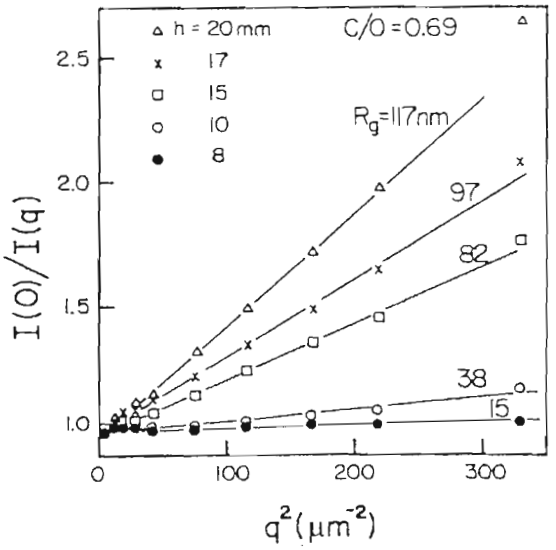

FIGURE 17 Guinier analysis of structure factor data in Figure 15. By Equation 34, I^{-1} vs. q^2 yields straight lines with slope $R_g^2/3$.

Figure 16 shows data for $R_g = 0.5\mu$ which, because of this large size, has qR_g sufficiently large so that the asymptotic q^{-D} dependence can be seen. A good rule of thumb is that the power law regime does not begin until $qR_g \gtrsim 5$, hence data below this limit should not be used in an asymptotic analysis for D (i.e., finding D from the slope of log S(q) vs. log q). A good method of analysis is to find R_g via inverse intensity vs. q^2, as in Figure 17, and then to use this value while fitting to

the structure factor with the fractal dimension D being the only fit parameter. Our opinion is that the Gaussian cutoff-derived structure factor is the best for this, and one must include a realistic, finite width size distribution.

For soot or any other strongly absorbing material with a complex refractive index, a complete morphological characterization to determine average R_g, N, a, and D can be made with *in situ* light scattering.[33] The technique involves combining optical structure factor measurements and absolute scattering and extinction measurements. From Equations 8 and 32, the scattered intensity at small angles such that S(q) = 1 is

$$I_{scat} = nN^2k^4a^6F(m) \tag{40}$$

From Equations 14, 33, 17, and 20, the turbidity is

$$\tau = nN\,4\pi ka^3E(m) \tag{41}$$

A ratio eliminates n; thus,

$$\frac{I_{scat}}{\tau}\cdot\frac{4\pi}{k^3} = N\,a^3F(m)/E(m) \tag{42}$$

Measurement of absolute I_{scat} is achieved via calibration of scattering from gases or liquids of known Rayleigh ratio with knowledge of the particle refractive index. Equation 42 allows for determination of the scattering/extinction radius:

$$R_{SE}^3 = N\,a^3 \tag{43}$$

which is the volume-equivalent sphere radius.

Now consider again Equation 31:

$$N = k_o\left(R_g/a\right)^D \tag{31}$$

Equations 31 and 43 can be solved for N or a in terms of the measurable R_{SE}, R_g, and D:

$$a = \left(R_{SE}^3/k_oR_g^D\right)^{1/(3-D)} \tag{44a}$$

$$N = k_0^{3/3-D}\left(R_g/R_{SE}\right)^{3D/(3-D)} \tag{44b}$$

Uncertainties arise from three sources, the value of k_o, the index of refraction, and, not shown above, correction to Equation 44 for a polydisperse system. The reader should consult the literature for a more detailed explanation.[33]

The validity of the fractal optics embodied in Equations 32 and 33 has been investigated both theoretically and experimentally. Nelson[31] studied the effects of intracluster multiple scattering for clusters of both D = 1.8 and 2.5 and N on the order of 100. For D = 1.8, corrections to Equations 32 and 33 are on the order of a few to several percent. On the other hand, for D = 2.5 significant deviations occurred. Lu and Sorensen[51] found that the depolarization ratio, ρ, of light scattered from fractal soot clusters went as $\rho \sim N^{-0.6}$ and was fairly small, on the order of a percent and less,

and they were able to explain these observations theoretically. In unpublished work, we used this theory to find deviations from Equations 32 and 33 to be on the order of 5 and 10%, respectively, for soot clusters with a monomer size parameter equal to 0.2.

Cai, Lu, and Sorensen[52] used the combined optical structure factor and scattering/extinction measurements embodied in Equation 44 to measure R_g, N, a, and D for soot clusters *in situ* in a CH_4/O_2 premixed flame. Soot was then collected by thermophoresis onto TEM grids. Digital analysis of the electron microscope pictures yielded the same four morphological parameters. R_g and D agreed very well, to within 5%. Greater variation was obtained for N and a, but the light scattering and TEM values were consistent. Errors are incurred through poor knowledge of the size distribution and the soot refractive index. This latter uncertainty, which can be a factor of about two, has plagued combustion soot optical diagnostics for some time. Koylu and Faeth[53,54] have made similar comparisons but with soot collected from a wide variety of flames. Again, the conclusion was that fractal optics is pretty good, certainly better than Rayleigh or volume-equivalent sphere approximations, but the major source of uncertainty is the soot refractive index.

ACKNOWLEDGMENTS

My interaction with both my former students, J. Cai and N. Lu, and current students, C. Oh, H. Huang, and R. Pande, has helped shape the form of this review. This work has been supported by grants from the National Science Foundation and National Institutes of Standards and Technology.

APPENDIX A. CROSS-SECTIONS

Differential Cross-Sections

The differential scattering cross-section, $d\sigma/d\Omega$, describes the power scattered, P_{scat}, per unit solid angle, Ω, (watts/steradian) for an incident intensity (watts/meter^2) I_o:

$$\frac{P_{scat}}{\Omega} = \frac{d\sigma}{d\Omega} I_o \tag{A1}$$

Thus, the units of $d\sigma/d\omega$ are meter^2/steradian.

The scattered intensity is the scattered power per unit area of detection:

$$I_{scat} = P_{scat} / A \tag{A2}$$

The solid angle subtended by the detector a distance, r, from the scatterer is

$$\Omega = A / r^2 \tag{A3}$$

Thus, from Equations A1, A2, and A3 one obtains:

$$I_{scat} = I_o \frac{d\sigma}{d\Omega} \frac{1}{r^2} \tag{A4}$$

One obtains the well known $1/r^2$ dependence due to the geometry of space as described by Equation A3.

The Total Cross-Section

The total scattering cross-section is found by integration of the differential cross-section over the complete solid angle:

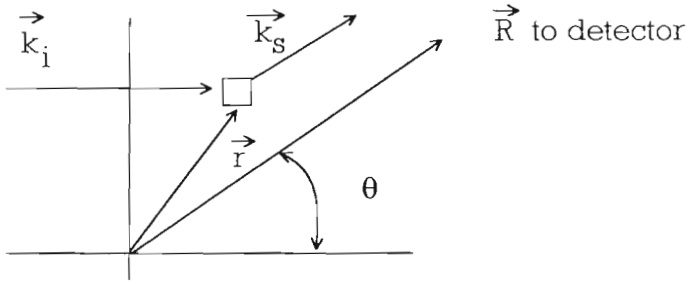

FIGURE 18 Light with incident wave vector, $\vec{k}_i$, scatters from an element at $\vec{r}$ into a direction $\vec{k}_s$ directed toward the detector at scattering angle θ and great relative distance.

$$\sigma = \int_{4\pi} \frac{d\sigma}{d\Omega} d\Omega \tag{A5}$$

This integral must include polarization effects (see main text). The differential element $d\Omega$ in three-dimensional Euclidean space is (see Figure 1 for the polar coordinates θ and ϕ):

$$d\Omega = d\theta d(\cos\phi) \tag{A6}$$

Efficiencies

The scattering or absorption efficiency is a dimensionless ratio of the total cross to the projected (onto a plane) area of the scatterer:

$$Q_{\text{scat or abs}} = \frac{\sigma_{\text{scat or abs}}}{A_{\text{proj}}} \tag{A7}$$

For a sphere of radius a:

$$A_{\text{proj}} = \pi a^2 \tag{A8}$$

These quantities are physically intuitive because they compare the optical cross-section to the geometric cross-section. If light was not a wave (e.g., solely a particle), the sum of the scattering and absorption efficiencies would be unity.

APPENDIX B. THE SCATTERING WAVE VECTOR

Consider a scalar electromagnetic field with incident wave vector $\vec{k}_i$ incident upon a scattering element at $\vec{r}$ as in Figure 18. The incident field at $\vec{r}$ is

$$E_i \propto e^{i\vec{k}_i \cdot \vec{r}} \tag{B1}$$

where we keep track of phase information only. The field scatters toward the detector in the direction $\vec{k}_s$ where $\vec{k}_s$ is the scattered wave vector. We assume elastic scattering, i.e.,

$$\left|\vec{k}_i\right| = \left|\vec{k}_s\right| = \frac{2\pi}{\lambda} \tag{B2}$$

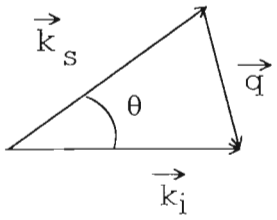

FIGURE 19 Relationship between the incident $\vec{k}_i$ and scattered $\vec{k}_s$ wave vectors, the scattering angle, θ, and the scattering wave vector, $\vec{q}$.

The field at the detector, which is at $\vec{R}$, is

$$E(\vec{R}) \propto E(\vec{r})e^{i\vec{k}_s(\vec{R}-\vec{r})} \tag{B3}$$

Substitution of Equation B1 into Equation B3 yields:

$$E(\vec{R}) \propto e^{ik_s \cdot R} e^{i(\vec{k}_i - \vec{k}_s)\cdot\vec{r}} \tag{B4}$$

The second term of Equation B4 shows that the phase at the detector is a function of the position of the scattering element and the vector:

$$\vec{q} = \vec{k}_i - \vec{k}_s \tag{B5}$$

This vector, $\vec{q}$, is called the scattering wave vector. Its direction is in the scattering plane from $\vec{k}_s$ to $\vec{k}_i$, as shown in Figure 19. From Figure 19 and the elasticity condition (Equation B2), the magnitude of is $\vec{q}$ is

$$q = 2k_i \sin\theta/2 \tag{B6a}$$

$$= 4\pi\lambda^{-1}\sin\theta/2 \tag{B6b}$$

where θ is the scattering angle.

The importance of q is that its inverse, q^{-1}, represents the length scale of the scattering experiment. This follows from the second term in Equation B4, which can now be written as:

$$e^{i\vec{q}\cdot\vec{r}} \tag{B7}$$

As we have seen, expression B7 gives the phase at the detector due to a scattering element at $\vec{r}$. The scattering due to an object will be the sum of such terms, weighted by the scattering density, over the extent of the object. The key point is that during this sum, the phase expression B7 will not vary significantly if the range of $\vec{r}$ is small compared to q^{-1}. Thus, the scattered phase is not sensitive to the overall extent of the object. One might say that the scattering cannot "see" the object.

Application of this concept to scattering for a particle of extent a implies that if $a << q^{-1}$ (i.e., $qa << 1$), the scattering cannot see the morphology of the particle. Furthermore, if q varies but qa remains less than unity there will be no dependence on q, i.e., no scattering angle dependence. This is the Rayleigh regime for any size particle.

Another consequence of the phase term (Equation B7) is that if $qa << 1$, the fields from the scattering elements add coherently. For an object in three dimensions, this coherent addition occurs for all three dimensions, and the three dimensions add coherently. Thus, the scattered field will be proportional to the amount of matter in the object which is proportional to the volume, V, of a dense particle or the number of monomers per cluster, N, of a ramified object. Since intensity is the field squared, one obtains V^2 or N^2 dependencies.

In summary, q^{-1} is the length scale or resolution limit of a scattering experiment; therefore, the dimensionless product, qa, where a is a measure of the extent of an object, determines the boundary of the Rayleigh regime: If $qa << 1$, then $I \sim V^2$ or N^2 is not a function of θ, the Rayleigh regime; if $qa > 1$, then $I = I(\theta)$.

REFERENCES

1. van de Hulst, H. C., *Light Scattering by Small Particles*, Dover, New York, 1981.
2. Kerker, M., *The Scattering of Light and Other Electromagnetic Radiation*, Academic Press, New York, 1969.
3. Bohren, C. F. and Huffman, D. R., *Absorption and Scattering of Light by Small Particles*, John Wiley & Sons, New York.
4. Minneart, M. G. J., *Light and Color in the Outdoors*, Springer-Verlag, New York, 1993.
5. Hecht, E., *Optics*, Addison-Wesley, Reading, MA, 1990.
6. Jones, A. R., Electromagnetic wave scattering by assemblies of particles in the Rayleigh approximation, *Proc. Roy. Soc. Lond. Ser.*, A366, 111, 1979.
8. Fuller, K. A. and Kattawar, G. W., Consummate solution to the problem of classical electromagnetic scattering by ensembles of spheres. I. Linear chains, *Opt. Lett.*, 13, 90, 1988.
9. Fuller, K. A. and Kattawar, G. W., Consummate solution to the problem of classical electromagnetic scattering by ensembles of spheres. II. Clusters of arbitrary configuration, *Opt. Lett.*, 13, 1063, 1988.
11. Fuller, K. A., Scattering and absorption cross-sections of compounded spheres. I. Theory for external aggregation, *J. Opt. Soc. Am.*, A11, 3251, 1994.
12. Fuller, K. A., Scattering and absorption cross-sections of compounded spheres. II. Calculations for external aggregation, *J. Opt. Soc. Am.*, A12, 881, 1995.
13. Chen, H. Y., Iskander, M. F., and Penner, J. E., Light scattering and absorption by fractal agglomerates and coagulations of smoke aerosols, *J. Modern Opt.*, 2, 171, 1990.
15. Ku, J. C. and Shim, K. H., Optical diagnostic and radiative properties of simulated soot agglomerates, *Am. Soc. Mech. Eng. Heat Transfer*, 113, 953, 1992.
16. Ku, J. C. and Shim, K. H., A comparison of solutions for light scattering and absorption by agglomerated or arbitrary shaped particles, *Quant. Spectrosc. Radiat. Trans.*, 47, 201, 1992.
17. Mackowski, D. W., Analysis of radiative scattering for multiple sphere configurations, *Proc. Roy. Soc. Lond. Ser.*, A433, 599, 1991.
18. Mackowski, D. W., Calculation of total cross-sections of multiple-sphere clusters, *J. Opt. Soc. Am.*, 11, 2851, 1994.
19. Mackowski, D. W., Electrostatic analysis of radiative absorption by sphere clusters in the Rayleigh limit: application to soot clusters, *Appl. Opt.*, 34, 3535, 1995.
20. Quinten, M. and Kreibig, U., Absorption and elastic scattering of light by particle aggregates, *Appl. Opt.*, 32, 6173, 1993.
21. Mandelbrot, B., *The Fractal Geometry of Nature*, W. H. Freeman, San Franciso, CA, 1983.
22. Forrest, S. R. and Witten, T. A., Long-range correlations in smoke-particle aggregates, *J. Phys.*, A12, L109, 1979.
23. Family, F. and Landau, D. P., Eds., *Kinetics of Aggregation and Gelation*, North-Holland, Amsterdam, 1984.
24. Stanley, H. E. and Ostrowsky, N., Eds., *On Growth and Form*, Nijhoff, Boston, MA, 1986.
25. Jullien, R. and Botet, R., *Aggregation and Fractal Aggregates*, World Scientific, Singapore, 1987.
26. Berry, M. V. and Percival, I. C., Optics of fractal clusters such as smoke, *Opt. Acta*, 33, 577, 1986.
27. Freltoft, T., Kjems, J. K., and Sinha, S. K., Power-law correlations and finite-size effects in silica particle aggregates studied by small-angle neutron scattering, *Phys. Rev. B*, 33, 269, 1986.

28. Teixeira, J., in *On Growth and Form*, Stanley, H. E. and Ostrowski, N., Eds., Nijhoff, Boston, MA, 1986.
29. Martin, J. E. and Hurd, A. J., Scattering from fractals, *J. Appl. Cryst.*, 20, 61, 1987.
30. Mountain, R. D. and Mulholland, G. W., Light-scattering from simulated smoke agglomerates, *Langmuir*, 4, 1321, 1988.
31. Nelson, J., Test of a mean field theory for the optics of fractal clusters, *J. Mod. Opt.*, 36, 1031, 1989.
32. Singham, S. B. and Borhen, C. F., Scattering of unpolarized and polarized light by particle aggregates of different size and fractal dimension, *Langmuir*, 9, 1431, 1993.
33. Sorensen, C. M., Cai, J., and Lu, N., Light scattering measurements of monomer size, monomers per aggregate, and fractal dimension for soot aggregates in flames, *Appl. Opt.*, 31, 6547, 1992.
34. Cai, J., Lu, N., and Sorensen, C. M., Analysis of fractal cluster morphology parameters: structural coefficient and density autocorrelation function cutoff, *J. Coll. Interfaces*, 171, 470, 1995.
35. Wu, M. K. and Friedlander, S. J., Note on the power law equation for fractal-like aerosol agglomerates, *J. Coll. Interface Sci.*, 159, 246, 1993.
36. Koylu, U. O., Faeth, G. M., Farias, T. H., and Carvalho, M. G., Fractal and projected structural properties of soot aggregates, *Combust. Flame*, 100, 621, 1995.
37. Guinier, A., *X-Ray Diffraction in Crystals, Imperfect Crystals, and Amorphous Bodies*, Dover, New York, 1994.
38. Sorensen, C. M., Cai, J., and Lu, N., Test of structure factors for describing light scattering from fractal soot aggregates, *Langmuir*, 8, 2064, 1992.
39. Pearson, A. and Anderson, R. W., Long-range pair correlation and its role in small-angle scattering from fractals, *Phys. Rev. B*, 48, 5865, 1993.
40. Yanwei, Z. and Meriani, S., Scaling functions for the finite-size effect in fractal aggregates, *J. Appl. Cryst.*, 27, 782, 1994.
41. Schaefer, D. W., Martin, J. E., Wiltzius, P., and Cannell, D. S., Fractal geometry of colloidal aggregates, *Phys. Rev. Lett.*, 52, 2371, 1984.
42. Abramowitz, A. and Stegun, I. A., Eds., *Handbook of Mathematical Functions*, Dover, New York, 1972.
43. Hurd, A. J. and Flower, W. L., *In situ* growth and structure of fractal solica aggregates in a flame, *J. Colloid Interface Sci.*, 122, 178, 1988.
44. Lin, M. Y., Klein, R., Lindsay, H. M., Weitz, D. A., Ball, R. C., and Meaking, P., The structure of fractal colloidal aggregates of finite extent, *J. Coll. Interface Sci.*, 137, 263, 1990.
45. Dobbins, R. A. and Megaridis, C. M., Absorption and scattering of light by polydisperse aggregates, *Appl. Opt.*, 30, 4747, 1991.
46. Jullien, R., From Guinier to fractals, *J. Phys. I (France)*, 2, 759, 1992.
47. Vaglieco, B. M., Beretta, F., and D'Alessio, A., *In situ* evaluation of the soot refractive index in the UV-visible from measurement of the scattering and extinction coefficients in rich flames, *Combust. Flame*, 79, 259, 1990.
48. Gangopadhyay, S., Elminyawi, I., and Sorensen, C. M., Optical structure factor measurements for soot particles in a premixed flame, *Appl. Opt.*, 30, 4859, 1991.
49. Tanford, C., *Physical Chemisty of Macromolecules*, Wiley, New York, 1961.
50. Cai, J., Lu, N., and Sorensen, C. M., Fractal cluster size distribution measurement using static light scattering, *J. Coll. Interface Sci.*, 174, 456, 1995.
51. Lu, N. and Sorensen, C. M., Depolarized light scattering from soot fractal aggregates, *Phys. Rev. E*, 50, 3109, 1994.
52. Cai, J., Lu, N., and Sorensen, C. M., Comparison of size and morphology of soot aggregates as determined by light scattering and electron microscope analysis, *Langmuir*, 9, 2861, 1993.
53. Koylu, U. O. and Faeth, G. M., Optical properties of soot in buoyant laminar diffusion flames, *J. Heat Trans.*, 116, 971, 1994.
54. Koylu, U. O. and Faeth, G. M., Optical properties of overfire soot in buoyant turbulent diffusion flames at long residence times, *Trans. Am. Soc. Mech. Eng.*, 116, 152, 1994.